^{21}Ne from ^{12}C(^{10}B,p)

S. Mordechai* and H. T. Fortune
Physics Department, University of Pennsylvania, Philadelphia, Pennsylvania 19104
(Received 8 April 1985)

The ^{12}C(^{10}B,p)^{21}Ne reaction has been investigated at an incident energy of 20 MeV. Complete angular distributions were measured in the angular range $\theta_{lab}=7.5°-161.25°$ using a multiangle spectrograph. Angular distributions for states in ^{21}Ne up to 6.75 MeV excitation are found to be symmetric around 90°. Results have been analyzed in terms of Hauser-Feshbach compound-nucleus calculations. A simple analysis of the angle-integrated cross sections versus $(2J+1)$ shows that the $(2J+1)$ rule holds for states with angular momenta up to $\frac{7}{2}$. States with higher J are significantly enhanced due to kinematical conditions. The Hauser-Feshbach calculations account fairly well for the high-J enhancement of σ_{tot}.

I. INTRODUCTION

The low-lying level structure of ^{21}Ne has been investigated extensively in the past,[1–7] predominantly via gamma decay with the reactions ^{18}O(α,nγ)^{21}Ne and ^{12}C(^{13}C,$\alpha\gamma$)^{21}Ne.[2] Gamma-decay schemes and lifetimes have been established for most bound states ($E_x \lesssim 6.8$ MeV). Most of the levels below 5 MeV excitation have been classified into rotational bands and can easily be understood[6,8] in terms of the Nilsson model for both negative and positive parity. However, above 5 MeV excitation, many states have only tentative spin and parity assignments[1] and the correspondence between experimental levels and Nilsson-model states is very uncertain. Shell-model calculations[9,10] in an $(sd)^5$ basis are also able to account for much of the experimental information on the positive-parity states.

In a previous study of the ^{12}C(^{10}B,d)^{20}Ne reaction at $E_{lab}=20.0$ and 20.5 MeV it was found[11] that core-excited states were selectively excited in the reaction, though to a lesser extent than in the ^{12}C(^{12}C,α)^{20}Ne reaction,[12] perhaps indicating some contribution from a direct-reaction mechanism which involves a transfer of eight nucleons.

The present work reports results of a study of the reaction ^{12}C(^{10}B,p)^{21}Ne. Little information is available on the mechanism of this reaction. Our choice of target was motivated by the large number of low-lying final states in ^{21}Ne which have known J^π.

II. EXPERIMENTAL PROCEDURE

The experiment was performed with a 20-MeV ^{10}B beam from the University of Pennsylvania Tandem Accelerator. The target was a 10 μg/cm^2 self-supporting foil of enriched (99.99%) ^{12}C. The use of such a thin target enabled good resolution, despite the large stopping power of ^{10}B ions. Outgoing protons were momentum analyzed with a multiangle spectrograph and recorded on Ilford $K5$ nuclear emulsion plates in the angular range of 3.75°–78.75° and 86.25°–161.25° in 15° steps. The total exposure was 15 000 μC. Mylar foil absorbers of variable thickness (0–0.63 mm) were placed in front of the focal plane to stop all ions heavier than protons.

Figure 1 shows two typical spectra measured at 18.75° and at 161.25° covering an excitation energy range of about 6.8 MeV. The overall energy resolution (full width at half maximum) was about 30 keV and arose primarily from energy loss of the ^{10}B ions in the target. Excitation energies were obtained from observed peak positions and

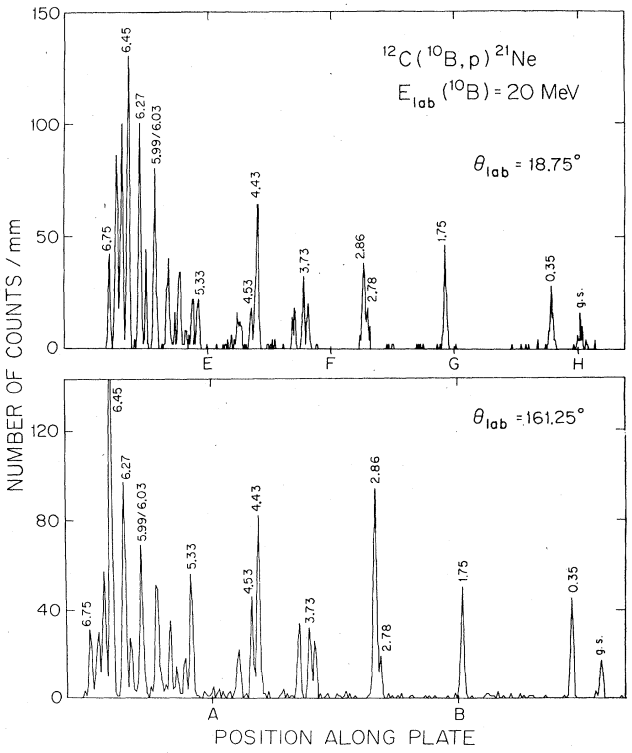

FIG. 1. Proton spectra from the ^{12}C(^{10}B,p)^{21}Ne reaction measured at 20 MeV incident energy and at laboratory angles of 18.75° (top) and 161.25° (bottom). Some of the levels in ^{21}Ne are indicated by their excitation energies. Index marks are 13.32 cm apart.

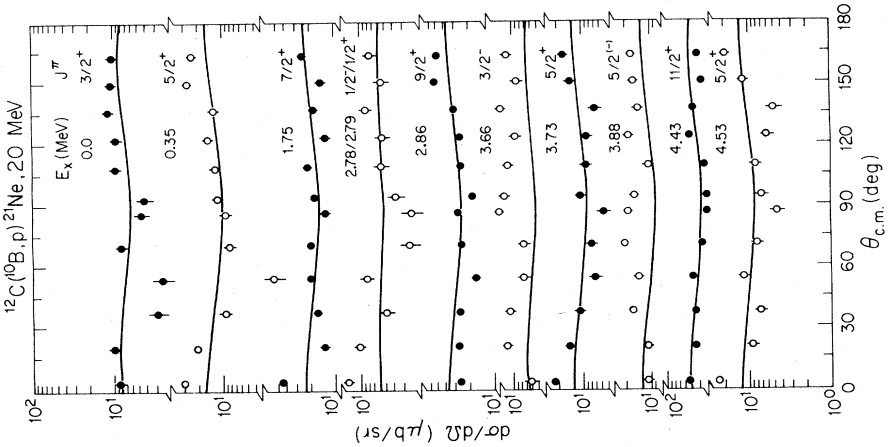

FIG. 2. Angular distributions for the ^{12}C(^{10}B,p)^{21}Ne reaction leading to levels between 0 and 4.5 MeV excitation in ^{21}Ne. Curves are the results of a statistical model calculation using the code STATIS.

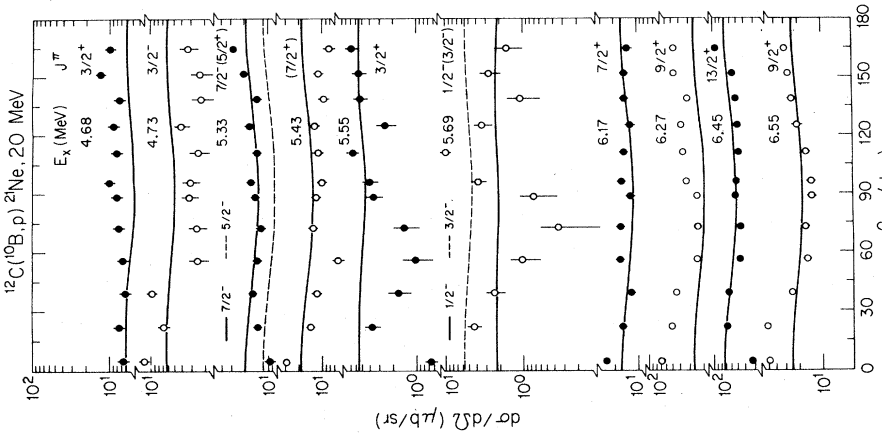

FIG. 3. Same as Fig. 2 but for 4.6–6.5 MeV excitation.

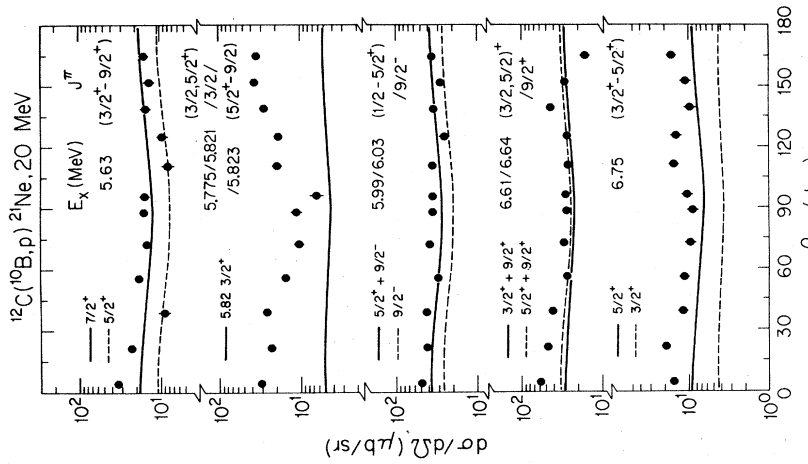

FIG. 4. Angular distributions for five additional levels, doublet or triplet levels with unknown spins between 5.6 and 6.7 MeV excitation.

TABLE I. Results from the $^{12}C(^{10}B,p)^{21}Ne$ reaction at 20 MeV.

Present E_x (keV)	Literature[a] E_x (keV)	J^π	σ_{tot} (μb) 0°–90°	σ_{tot} (μb) 0°–180°	$\frac{\sigma(0°-90°)}{\sigma(90°-180°)}$	$\frac{\sigma(0°-180°)^f}{2J+1}$ (μb)	$R \pm \Delta R^g$	J limit
0	0	$\frac{3}{2}^+$	34.5	90.7	0.61	22.7	1.35±0.49	0.86–1.84
353±6	350.72	$\frac{5}{2}^+$	60.0	156.9	0.62	26.2	2.71±0.85	1.86–3.56
1752±6	1745.6	$\frac{7}{2}^+$	114.9	228.1	1.02	28.5	4.16±1.24	2.92–5.40
	2788.5	$\frac{1}{2}^-$						
2806±5			35.4	71.8	0.97	18.0[d]	0.47±0.26	0.21–0.73
	2796.1	$\frac{1}{2}^+$						
2875±5	2865.6	$\frac{9}{2}^+$	152.2	341.5	0.80	34.2	4.45±0.21	4.24–4.66
3670±5	3662.1	$\frac{3}{2}^-$	61.7	134.1	0.85	33.5	2.24±0.73	1.51–2.97
3742±4	3733.7	$\frac{5}{2}^+$	57.4	120.5	0.91	20.1	1.96±0.65	1.31–2.61
3886±5	3882.9	$\frac{5}{2}^{(-)}$	106.6	202.4	1.11	33.7	3.64±1.10	2.54–4.74
4438±6	4432.2	$\frac{11}{2}^+$	260.5	510.8	1.04	42.6	5.51±0.25	5.26–5.76
4533±5	4524.2	$\frac{5}{2}^+$[b]	56.8	109.0	1.09	18.2	1.73±0.59	1.14–2.32
4709±7	4683.6	$\frac{3}{2}^+$[b]	45.9	105.1	0.78	26.3	1.65±0.57	1.08–2.22
4757±6	4725.7	$\frac{3}{2}^-$	30.4	49.2	1.63	12.3	0.51±0.27	0.24–0.78
5347±4	5334	$\frac{7}{2}^-(\frac{5}{2}^+)$[b]	87.7	195.8	0.81	24.5[e]	3.50±1.06	2.44–4.56
5442±4	5430.0	$(\frac{7}{2}^+)$[b]	74.3	142.8	1.08	17.9	2.42±0.78	1.64–3.20
5552±5	5550[h]	$\frac{3}{2}^+$	13.7	44.8	0.44	11.2	0.42±0.24	0.18–0.66
5637±6	5629.4	$(\frac{3}{2}^+ - \frac{9}{2}^+)$	104.5	182.7	1.34	18.3–45.7	3.24±0.99	2.25–4.23
5707±10	5690	$\frac{1}{2}^-(\frac{3}{2}^-)$[b]	9.7	37.3	0.35	18.65[i]	0.26±0.20	0.06–0.46

the known magnet calibration. Some of the levels in ^{21}Ne are indicated in the figure by their excitation energies. In Table I all states are listed by their excitation energies along with the values from the literature. Absolute cross sections were obtained from the measured target thickness and integrated beam current. The uncertainty in the overall cross-section scale is estimated at 20%.

III. RESULTS

Angular distributions were extracted for all observed states in ^{21}Ne up to an excitation energy of 6.75 MeV. They are displayed in Figs. 2–4 and compared with results of Hauser-Feshbach (HF) statistical compound-nucleus calculations using the code STATIS.[13] Details of these calculations are given in Sec. IV B. Figure 2 displays the data for the ground state (g.s.) and the excited states up to 4.53 MeV in the order of excitation energy. Transitions to states between 4.68 and 6.55 MeV excitation are shown in Fig. 3. Figure 4 contains the data for five additional levels, doublet or triplet levels between 5.6 and 6.7 MeV excitation with previously undetermined spins.

Values of σ_{tot} obtained by integrating all points in the angular distributions in the ranges (0°–90°) and (90°–180°) are listed in Table I. The table also gives the ratios $\sigma_{tot}(0°-90°)/\sigma_{tot}(90°-180°)$ and $\sigma_{tot}(0°-180°)/(2J+1)$. The integrated cross sections (CS's) $\sigma_{tot}(0°-180°)$ are plotted versus $2J+1$ (where J is the spin of the final state) in Fig. 5.

Simple features of the results (both the integrated and the differential CS's) indicate that the (^{10}B,p) reaction at 20 MeV proceeds predominantly via pure compound-nucleus formation. The angular distributions shown in Figs. 2–4 are symmetric around 90° for most of the transitions. Similarly the ratio $\sigma_{tot}(0°-90°)/\sigma_{tot}(90°-180°)$ is near to or slightly smaller than unity for most states—indicating that the CS's at backward angles are equal or somewhat larger than those at the forward angles. The

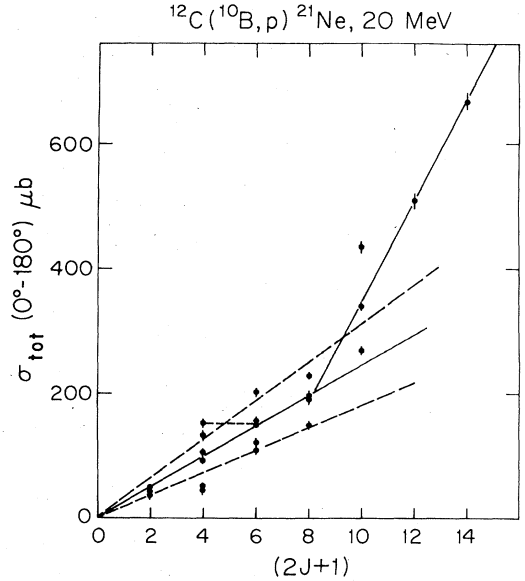

FIG. 5. Plot of $\sigma_{tot}=2\pi\int_{0°}^{180°}\sigma(\theta)\sin\theta\, d\theta$ vs $(2J+1)$ for all levels in ^{21}Ne below 6.7 MeV which have a known spin.

TABLE I. (*Continued*).

Present E_x (keV)	Literature[a] E_x (keV)	J^π	σ_{tot} (μb) 0°—90°	0°—180°	$\frac{\sigma(0°-90°)}{\sigma(90°-180°)}$	$\frac{\sigma(0°-180°)^f}{2J+1}$ (μb)	$R\pm\Delta R^g$	J limit
	5775	$(\frac{3}{2},\frac{5}{2}^+)$						
5822±5	5821	$\frac{3}{2}$	107.0	238.2	0.82	11.9—17.0	3.37±1.03	2.34—4.40
	5823	$(\frac{5}{2}^+-\frac{9}{2})$						
	5992.9	$(\frac{1}{2}-\frac{5}{2}^+)$						
6026±12			235.4	438.8	1.16	27.4—36.6	7.97±2.25	5.72—10.22
	6030.7	$\frac{9}{2}^{-b}$						
6180±6	6169	$\frac{7}{2}^{+b}$	97.6	189.3	1.06	23.7	3.37±1.03	2.34—4.40
6273±6	6265.1	$\frac{9}{2}^{+c}$	205.6	439.2	0.88	43.9	5.06±0.23	4.83—5.29
6463±8	6446.6	$\frac{13}{2}^{+c}$	329.6	669.6	0.97	47.8	6.50±0.29	6.21—6.79
6562±6	6553	$\frac{9}{2}^{+b}$	142.4	269.4	1.12	26.9	4.0 ±0.19	3.81—4.19
	6605	$(\frac{3}{2},\frac{5}{2})^{+b}$						
6648±7			214.2	396.2	1.18	24.9—28.3	7.10±2.02	5.08—9.12
	6642	$\frac{9}{2}^{+b}$						
6756±8	6747.4	$(\frac{3}{2}^+-\frac{5}{2}^+)^c$	72.4	151.3	0.92	25.2—37.8	2.59±0.82	1.77—3.41

[a]Reference 1.
[b]Reference 2.
[c]Reference 3.
[d]$\sigma_{tot}(0°-180°)/\Sigma(2J+1)$.
[e]Assuming the 5.334 MeV state has $J=\frac{7}{2}$.
[f]For states with unknown spins upper and lower limits of $\sigma_{tot}(0°-180°)/(2J+1)$ are calculated based on the reported tentative spins.
[g]$R=[\sigma_{tot}(0°-180°)/48.9-\frac{1}{2}]$ for states with integrated CS's less than 250 μb. For states with $\sigma_{tot}>250$ μb, R has been calculated using the relation $R=[\sigma(0°-180°)+451.3]/160.18-\frac{1}{2}$.
[h]In Ref. 1 an additional close state has been reported at 5525.0 with $(\frac{3}{2}^+-\frac{11}{2}^+)$. According to Ref. 3 this level does not exist; we find no evidence for it.
[i]Assuming $J^\pi=\frac{1}{2}^-$ for this state. According to Ref. 1 there is an additional state at 5682.8 with $(\frac{3}{2}^+,\frac{7}{2})$. There is no evidence for its existence either in the present work or in Ref. 3.

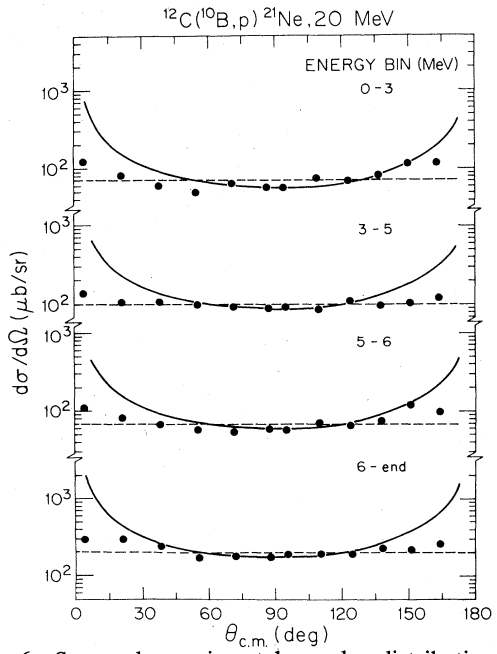

FIG. 6. Summed experimental angular distributions in the energy ranges: 0—3, 3—5, 5—6, and 6—end MeV. Solid and dashed curves are $1/\sin\theta$ and $\sigma(\theta)=$const fits to the data normalized to give the experimental integrated cross sections.

ratio $\sigma_{tot}(0°-180°)/(2J+1)$ presented in the seventh column of Table I is nearly constant for states with integrated CS's less than 250 mb. The scatter in $\sigma_{tot}(0°-180°)/(2J+1)$ is indicated in Fig. 5. The solid and dashed lines shown with the data for states with low J are the least squares linear fit plus and minus the standard deviation.

Figure 6 shows the summed experimental angular distributions in the energy ranges: 0—3, 3—5, 5—6, and 6—6.75 MeV. The solid and dashed curves are $1/\sin\theta$ and $\sigma(\theta)=$const fits to the data, respectively, normalized to give the exact summed experimental integrated CS's for the states in the given energy bin. Both curves fit the data very well at the intermediate angular range, and at the extreme forward and backward angles the data fall in between the two curves, with some preference for the isotropic assumption.

IV. ANALYSIS AND DISCUSSION

A. Analysis of the integrated cross sections

If the $(2J+1)$ rule were to hold for the compound nucleus[14] (CN), then we can express the angle-integrated

CS's as follows:

$$\sigma_{\text{tot}}(0°-180°)=\int_{0°}^{180°}(d\sigma/d\Omega)d\Omega$$
$$=\sigma_{\text{CN}}(2J+1)\ .$$

A least squares linear fit to the data (Fig. 5) yields $\sigma_{\text{CN}}=(24.5\pm6.5)$ μb for states with integrated CS's less than 250 μb. States with $J=\frac{9}{2}$, $\frac{11}{2}$, and $\frac{13}{2}$ have a larger ratio of $\sigma_{\text{tot}}/(2J+1)$. A fit of their integrated CS's vs $(2J+1)$ yields:

$$\sigma_{\text{tot}}(0°-180°)=-451.3+80.09(2J+1)\ \mu\text{b}\ ,$$

i.e., the slope is about three times that for low J. Only well-resolved single states with previously known spins have been included in the above fits. There is some evidence that the ratio $\sigma_{\text{tot}}/(2J+1)$ may be different for positive- and negative-parity states.[15,16] However, in the present study we observe no systematic difference between results for positive and negative parities and therefore the same analysis is carried out for both throughout the paper.

We can now use the approximate relationship between σ_{tot} and $(2J+1)$ to make inferences concerning spins of other states or to set upper and lower limits on their values. We define a quantity R:

$$R=\tfrac{1}{2}(\sigma_{\text{tot}}/24.45-1)$$

for states with $\sigma_{\text{tot}}\leq 250$ μb and,

$$R=\tfrac{1}{2}[(\sigma_{\text{tot}}+451.3)/80.09-1]$$

for states with $\sigma_{\text{tot}}>250$ μb. The calculated values of R are listed in Table I together with the corresponding J limits. For most single states the previously known spins fall within our J limits, indicating the validity of the method. Some deviations arise for unresolved doublets. This, for example, seems to be the case for the state at 5.822 MeV for which the predicted J limit is too high. For states with previously undetermined spins, our results can set a higher and lower limit on their possible spins. The state at 5.334 MeV $[\frac{7}{2}^-\ (\frac{5}{2}^+)]$ apparently has $J^\pi=\frac{7}{2}^-$. The state at 5.629 MeV has a reported tentative spin of $(\frac{3}{2}^+-\frac{9}{2}^+)$. Our results favor $J=\frac{5}{2}$ or $\frac{7}{2}$ for its spin. The 5.690-MeV state with $J^\pi=\frac{1}{2}^-\ (\frac{3}{2}^-)$ has a J limit of 0.06—0.46, thus we support the $\frac{1}{2}^-$ assignment. The 6.747-MeV state, with tentative spin of $(\frac{3}{2}^+-\frac{5}{2}^+)$, has J limits of 1.77—3.41—thus favoring the $J=\frac{5}{2}$ possibility.

Figure 7 shows a graph of $\Sigma\sigma_{\text{tot}}(0°-180°)/\Sigma(2J+1)$ versus excitation energy plotted in 1 MeV energy bins. Only states with well-known spins have been included in the figure. The data show an almost constant ratio of $\Sigma\sigma_{\text{tot}}/\Sigma(2J+1)$ over the range 0—5 MeV excitation as would be expected for a statistical compound mechanism. However, the higher two bins deviate from the constant ratio by about 30%. This deviation may arise either from the fact that many states with unknown spins, doublet or triplet of states, have been omitted from the sum, or due to the enhanced CS's observed for high-spin states due to kinematical conditions which will be discussed in subsection B. The numbers shown in parentheses in the figure denote the number of states included in the sum for each of the energy bins. The solid and dashed lines in the 5—6 MeV bin correspond to the two spin possibilities for the 5.334-MeV state as indicated in Table I.

Figure 8 shows a graph of $\langle\sigma_{\text{tot}}(J)\rangle$ vs $(J+\frac{1}{2})^2$ and $(J+\frac{1}{2})$ for all states with known J under 6.75 MeV excitation in ^{21}Ne, where $\langle\sigma_{\text{tot}}(J)\rangle$ is the averaged integrated CS for states with the same J. The data imply that $\log\langle\sigma_{\text{tot}}(J)\rangle$ is essentially linear when plotted versus $(J+\frac{1}{2})$ but not when plotted against $(J+\frac{1}{2})^2$. This result indicates that the averaged angle-integrated CS's are roughly proportional to $\exp[(J+\frac{1}{2})/2\sigma^2]$.

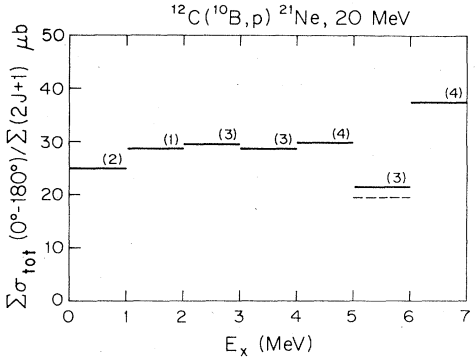

FIG. 7. $\Sigma\sigma_{\text{tot}}(0°-180°)/\Sigma(2J+1)$ vs E_x(MeV) plotted in 1 MeV excitation energy bins.

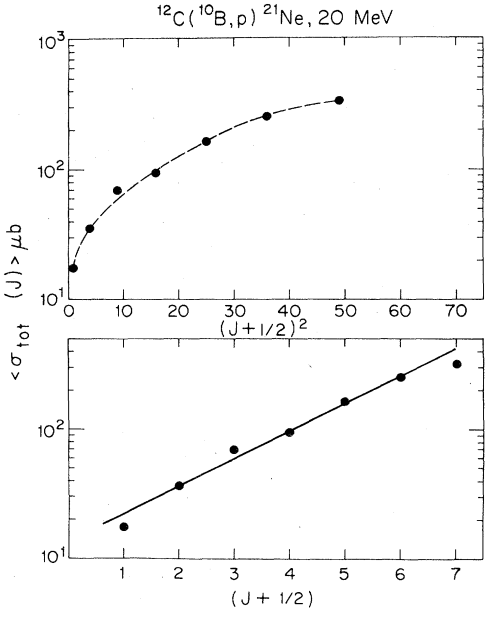

FIG. 8. Graph of $\langle\sigma_{\text{tot}}(J)\rangle$ vs $(J+\frac{1}{2})^2$ (top) and $(J+\frac{1}{2})$ (bottom) for states in ^{21}Ne.

B. Hauser-Feshbach calculations

Calculations of the compound-nuclear cross sections were performed using the computer code STATIS.[13] The details of such calculations are outlined in Refs. 17 and 18 and the formalism was taken from Refs. 19 and 20. The nuclear level density was taken to be of the form[21]

$$\rho(U,J)=\frac{(2J+1)}{12a^{1/4}(U+t)^{5/4}(2\sigma^2)^{3/2}}\times\exp[2(aU)^{1/2}]\exp\left[-\frac{(J+\frac{1}{2})^2}{2\sigma^2}\right],$$

where the nuclear temperature t is obtained from $U=at^2-t$ and $\sigma^2=\mathcal{I}t/h^2$. The rigid-body moment of inertia is

$$\mathcal{I}=(\tfrac{2}{5})mAR^2(1+0.31\beta+0.44\beta^2)$$

for $R=r_0A^{1/3}$, where m is the mass of a nucleon and A is the nuclear mass number. The excitation energy is defined as $U=E-b\delta$ where b is two for even-even, one for odd-even, and zero for odd-odd nuclei, and δ is the pairing energy taken to be 4.0 MeV.

The above equation has two unspecified parameters: level-density parameter and moment of inertia $\mathcal{I}$. We used the standard level-density parameter of 0.20 MeV^{-1} for the *sd* shell and $r_0=1.25$ fm, $\beta=0$ in the calculations of $\mathcal{I}$.

The transmission coefficients have been calculated using the ^{10}B optical-model parameters used recently for the system ^{12}C+^{11}B at $14\leq E_{\rm lab}\leq 54$ MeV (Ref. 22) and are listed in Table II. The fusion CS's have been measured for the systems ^{11}B+^{12}C and ^{10}B+^{13}C at many energies in the energy range $14\leq E_{\rm lab}\leq 54$ MeV.[22] From these measurements it is estimated that the fusion CS of ^{10}B+^{12}C at $E_{\rm lab}=20.0$ MeV ($E_{\rm c.m.}=10.91$ MeV) is about 800 mb. Therefore our method was to fix the calculated $\sigma_{\rm fus}$ at 800 mb by varying the critical angular momentum cutoff value. With $l_{\rm cr}=9$ the calculations yield $\sigma_{\rm fus}=812$ mb in close agreement with the above estimated value. This value of $l_{\rm cr}$ is also in agreement with the semiclassical estimate for ^{12}C+^{10}B at $E_{\rm lab}=20$ MeV. The calculated transmission coefficients from an optical model drop drastically for $l>l_{\rm cr}$, as do $\sigma_{\rm fus}$ and the total (^{10}B,p) reaction CS. Thus we used $l_{\rm cr}=9$ in all our HF calculations in the present work.

The results of the HF calculations are shown in Figs. 2–4 without any additional normalization factors. The calculations show that the proton channel exhausts about 56% of the total fusion CS and is the strongest decay channel of the compound nucleus. Except for the enhanced neutron decay predicted by the theory, the calculated total reaction CS for the various decay channels (e.g., p, α, d, ^{3}He, and t) show the expected *Qgg* dependence, namely the total CS's plotted against the Q value (*Qgg*) fall on a straight line on a logarithmic scale.

In general, the calculated angular distributions account fairly well for the magnitude of the data. However, for most states the measured angular distributions are more oscillatory than the calculated ones. The reason for this failure is not known, but may be connected with our use of a strongly absorptive potential in the entrance channel.

The unresolved doublet at 2.78/2.79 with $J^\pi=\frac{1}{2}^-/\frac{1}{2}^+$ is compared with the summed theoretical curves for the two individual states. The states at 5.33 MeV, $\frac{7}{2}^-$ ($\frac{5}{2}^+$), and 5.69 MeV, $\frac{1}{2}^-$ ($\frac{3}{2}^-$), have been compared with calculations for both possible spins (Fig. 3). Our results favor the previous tentative $\frac{7}{2}^-$ assignment for the first and a $\frac{1}{2}^-$ assignment for the second level (solid lines). Both assignments are also supported by the $(2J+1)$ analysis of the angle-integrated CS's discussed earlier (see Table I).

The states at 5.63 and 6.75 MeV have only tentative J^π limits in previous works. We compare the data for these states with calculations for two of the possible spin values. The solid lines which are the calculations assuming $\frac{7}{2}^+$ for the first and $\frac{5}{2}^+$ for the second state represent the best fit to the data. These tentative spin values are in good agreement with the J limits listed in Table I from the $2J+1$ analysis.

The cross section for the triplet of levels 5.775/5.821/5.823 with $(\frac{3}{2},\ \frac{5}{2}^+)/\frac{3}{2}/(\frac{5}{2}^+-\frac{9}{2})$ is compared with an HF curve for $J^\pi=\frac{3}{2}^+$ only. The experimental CS's for the triplet are everywhere above the theoretical curve due to the omission of the contributions of the other two members.

The unresolved doublet at 5.99/6.03 MeV $(\frac{1}{2}-\frac{5}{2}^+)/\frac{9}{2}^-$ is compared (Fig. 4) with HF curves calculated assuming $\frac{5}{2}^++\frac{9}{2}^-$ (solid) and $\frac{9}{2}^-$ alone (dashed). The solid line yields a better fit and supports the highest tentative ($\frac{5}{2}^+$) assignment for the 5.99 MeV state.

The doublet at 6.61/6.64 MeV $(\frac{3}{2},\ \frac{5}{2})^+/\frac{9}{2}^+$ is compared with the summed $\frac{3}{2}^++\frac{9}{2}^+$ curve (solid) and $\frac{5}{2}^++\frac{9}{2}^+$ curve (dashed), according to the two possible spin combinations. Both curves give equally good fits to the data, and thus we can make no choice between the two.

Figure 9 shows a graph of $\Sigma\sigma_{\rm tot}(0°-90°)/\Sigma(2J+1)$ and $\Sigma\sigma_{\rm tot}(90°-180°)/\Sigma(2J+1)$ vs J for states of known J in ^{21}Ne. The open circles represent the results of HF calculations. The solid line connects the theoretical points and just serves to guide the eyes. Two different features of the data should be emphasized. Firstly, we note the symmetry of $\Sigma\sigma_{\rm tot}$ around 90°, as the data points are roughly the

TABLE II. Entrance-channel optical-model parameters used in the Hauser-Feshbach statistical-model calculations in the present study.

System	V_0 (MeV)	r_0 (fm)	a_0 (fm)	W_0 (MeV)	r_i (fm)	a_i (fm)	r_c (fm)
^{12}C+^{10}B[a]	60.50	1.094	0.609	36.04	1.182	0.487	1.300

[a]Reference 22.

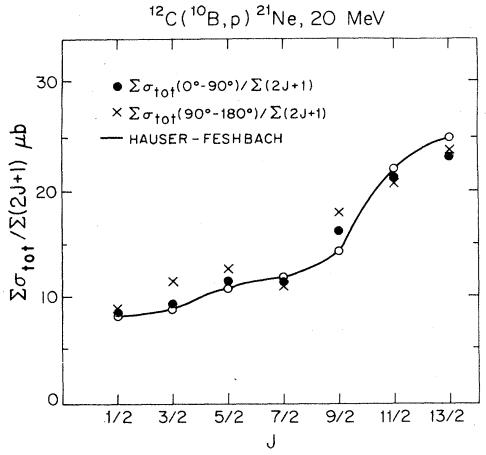

FIG. 9. Graph of $\Sigma\sigma_{tot}(0°-90°)/\Sigma(2J+1)$ and $\Sigma\sigma_{tot}(90°-180°)/\Sigma(2J+1)$ vs J for states in ^{21}Ne. The solid curve connects the Hauser-Feshbach statistical model predictions and serves to guide the eyes.

same in the forward and backward hemispheres. Secondly, the ratio $\Sigma\sigma_{tot}/\Sigma(2J+1)$ increases significantly with J (from a value about 9 μb for $J=\frac{1}{2}$ to a value of about 25 μb for $J=\frac{13}{2}$) indicating an enhanced population of final states in ^{21}Ne with high spins. This enhancement is due to kinematical rather than spectroscopic conditions and arises from the large mass difference between the incoming and outgoing particles. The incoming grazing angular momentum is about 9 whereas the outgoing is only about 3. Thus the L mismatch enhances the CS amplitude for high-spin states in the final nucleus. The integrated HF CS's reproduce the above enhancement quite well and account for the J dependence of the experimental angle-integrated CS's.

V. SUMMARY

In conclusion, the study of the reaction $^{12}C(^{10}B,p)$ has revealed that the reaction at 20 MeV is dominated by a compound-nucleus mechanism. A simple comparison of the angle-integrated cross sections with $(2J+1)$ shows that the $(2J+1)$ rule holds for states with spins up to $\frac{7}{2}$. States with higher J are significantly enhanced in the reaction due to the large L mismatch. We used the proportionality between σ_{tot} and $(2J+1)$ to make inferences concerning spins of states with previously undetermined J^{π}. The Hauser-Feshbach statistical compound calculations fail to reproduce the degree of oscillation in the differential cross sections for most states. However, they do account fairly well for the magnitude of the integrated CS's and reproduce the enhancement of the CS's at high J.

ACKNOWLEDGMENTS

We are grateful to M. Burlein and O. Kotwal for help in data analysis. This work was supported by the National Science Foundation.

*Present address: University of Texas at Austin, Austin, TX 78712. (Permanent address: Department of Physics, Ben-Gurion University of the Negev, Beer-Sheva, Israel.)

[1]P. M. Endt and C. van der Leun, Nucl. Phys. **A310**, 1 (1978).
[2]G. Andritsopoulos, W. N. Catford, E. F. Garman, D. M. Pringle, and L. K. Fifield, Nucl. Phys. **A372**, 281 (1981).
[3]H. Grawe, F. Heidinger, and K. Kändler, Z. Phys. A **280**, 271 (1977).
[4]J. C. Lawson and P. R. Chagnon, Phys. Rev. C **11**, 643 (1975).
[5]C. Rolfs, E. Kuhlmann, F. Reiss, and R. Kraemer, Nucl. Phys. **A167**, 449 (1971).
[6]C. Rolfs, H. P. Trautvetter, E. Kuhlmann, and F. Reiss, Nucl. Phys. **A189**, 641 (1972).
[7]H. T. Fortune, J. D. Garrett, and R. Middleton, Phys. Rev. C **19**, 1615 (1979); and references therein.
[8]E. Kuhlmann, A. Hoffmann, and W. Albrecht, Z. Phys. A **271**, 49 (1974).
[9]E. C. Halbert, J. B. McGrory, B. H. Wildenthal, and S. P. Pandya, in *Advances in Nuclear Physics,* edited by M. Baranger and E. Vogt (Plenum, New York, 1971), Vol. 4.
[10]W. Chung and B. H. Wildenthal (unpublished).
[11]H. T. Fortune, R. R. Betts, and R. Middleton, Phys. Rev. C **17**, 401 (1978).
[12]L. R. Greenwood, R. E. Segel, K. Raghunathan, M. A. Lee, H. T. Fortune, and J. R. Erskine, Phys. Rev. C **12**, 156 (1975).
[13]R. Stokstad, code STATIS, private communication.
[14]J. R. Powers, H. T. Fortune, and R. Middleton, Nucl. Phys. **A298**, 1 (1978).
[15]H. T. Fortune and J. N. Bishop, Nucl. Phys. **A293**, 221 (1977).
[16]H. T. Fortune and H. G. Bingham, Nucl. Phys. **A293**, 197 (1977).
[17]L. C. Dennis, A. Roy, A. D. Frawley, and K. W. Kemper, Nucl. Phys. **A359**, 455 (1981).
[18]H. V. Klapdor, H. Reiss, and G. Rosner, Nucl. Phys. **A262**, 157 (1976).
[19]T. D. Thomas, Annu. Rev. Nucl. Sci. **18**, 343 (1968).
[20]E. Vogt, in *Advances in Nuclear Science,* edited by M. Baranger and E. Vogt (Plenum, New York, 1968), Vol. I.
[21]R. W. Shaw, Jr., J. C. Norman, R. Vandenbosch, and J. C. Bishop, Phys. Rev. **184**, 1040 (1969).
[22]J. F. Mateja, A. D. Frawley, L. C. Dennis, K. Abdo, and K. W. Kemper, Phys. Rev. C **25**, 2963 (1982); J. F. Mateja, A. D. Frawley, L. C. Dennis, K. Abdo, and K. W. Kemper, Phys. Rev. Lett. **47**, 311 (1981).